Heat Flux

Josh Kraan

September 1, 2020

1 Introduction

In this document a new procedure to calculate heat flux using Cantera is detailed. The Feynman "Downsized 2" outputs are used for all example calculations.

The work here will make future heat flux calculations much easier. The effects of varying engine parameters can easily be seen without requiring the intermediate step of running them through NASA's CEA program, which is easy to misuse.

The heat flux calculated here will be used to look at the feasability of regenerative cooling, and could also be integrated with film cooling calulations being done by other team members.

2 Gas Properties

Combustion gas properties are commonly calculated using NASA's Chemical Equilibrium with Applications (CEA) [1] program, however this FORTRAN program is difficult to work with. Instead the combustion gas properties were calculated using Cantera as described by Youngblood [2].

Species included in the chemical equilibrium calculations were based off of those used in CEA and kerosene combustion models [3] as well as the availability of transport properties. The species that were included in this analysis are: RP-1, LOX, CO, CO2, H, H2, H2O, O, OH, and O2. RP-1 and LOX were modeled with the same stoichiometry and heat of formation as used in CEA. Cantera requires transport parameters for all species, so RP-1 and LOX were assigned placeholder values with the understanding that equilibrium solutions contain essentially zero concentration of these species.

Thermodynamic properties and Lennard-Jones transport parameters were taken from a high-temperature version of the GRI MECH 3.0 combustion mechanism [4] included with Cantera that has been extended from an upper temperature of 3500K to 6000K using the NASA Glenn Coefficients [5].

2.1 Property Evaluation

The procedure used to calculate the gas properties differs significantly from CEA. Instead of using a user-specified chamber pressure, the properties are calculated from engine geometry and flow rates.

The first step is the calculate the stagnation and throat properties, which are solved for together. At the throat of the engine, the following two conditions must be met [6]:

$$v = a \tag{1}$$

$$h_0 = h + \frac{v^2}{2} \tag{2}$$

The velocity and sound speed are calculated as follows:

$$v = \frac{\dot{m}}{A\rho} \tag{3}$$

$$a = \sqrt{\left(\frac{\partial p}{\partial \rho}\right)_s} \tag{4}$$

The partial derivative required to calculate the sounds speed is evaluated by perturbing the pressure at constant entropy [7]. If equilibrium expansion is used, the perturbed gas is equilibrated.

For a given stagnation pressure, the stagnation gas properties can be fully calculated as described by Youngblood. The throat conditions can then be solved for by varying the throat pressure isentropically until condition 1 is met. If condition 2 is met, the stagnation pressure is correct, if not, another stagnation pressure must be guessed. Two root finders were used to solve for the chamber and throat properties in this manner.

With the stagnation enthalpy known, the conditions at all other points of the engine can be solved for by varying the pressure isentropically until condition 2 is met. Both subsonic and supersonic solutions exist; specific solutions are forced by using the throat pressure to limit the solution range.

2.2 Frozen Boundary Layer Chemistry

CEA calculates "frozen" and "equilibrium" values for specific heat and thermal conductivity. Equilibrium values are taken to be the sum of the frozen value and a reaction term that accounts for chemical reactions occurring in the boundary layer. Equilibrium values for both are several times higher than frozen, and using the equilibrium values gives a calculated heat flux approximately 4.5 times higher (based on the Bartz equation).

Bartz [8, Page 46] discusses chemical reactions occurring in rocket engine boundary layers and the resulting increase in heat transfer. When dissociated species such as O, H, and OH are present in the free stream, they can cool against combustion walls and recombine exothermically in the boundary layer. Bartz notes that this effect would likely be maximum for a hydrogen and oxygen rocket at 100% combustion efficiency, yet the increase in heat flux over a frozen layer is shown to be only 32% and rapidly decreases with reduced combustion efficiency.

The presence of dissociated species is not insignificant for this engine, as can be seen in Figure 1. It is unclear why equilibrium values calculated by CEA are so high and reproducing them is difficult, so based off of the Bartz information the boundary layer was considered to be chemically frozen.

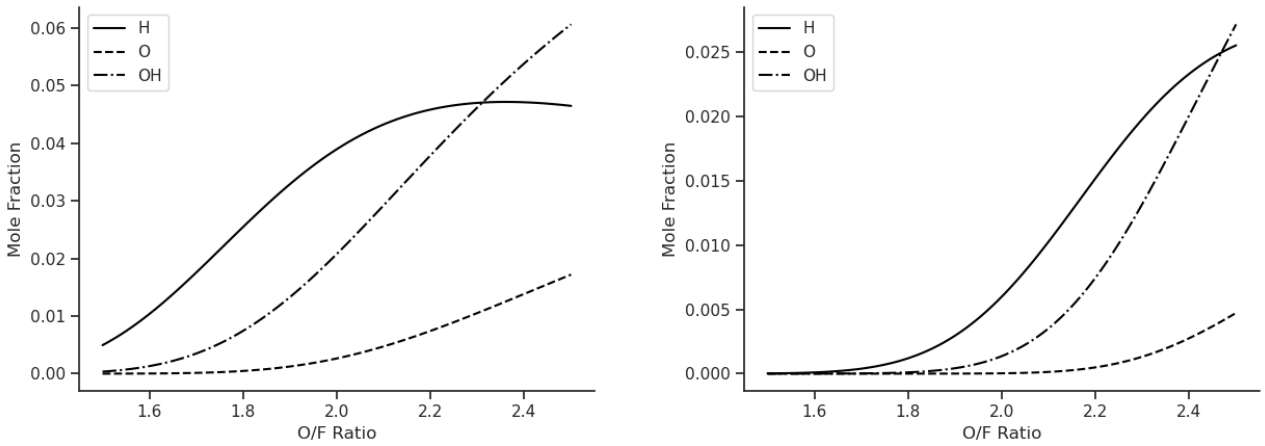

(a) Chamber (b) Nozzle

Figure 1: Dissociated species with equilibrium expansion, OF = 2.29.

2.3 Frozen Contraction and Expansion

Through the contraction and expansion of the engine, combustion gas can be considered to either be in equilibrium (mole fractions change along length of engine) or the composition could be frozen. Both methods were implemented, but this was found to make little difference to heat flux calculations.

2.4 Property Comparison

Table 1: Cantera and CEA comparison, equilibrium expansion, OF = 2.29.

	Stagnation		Throat		Exit	
	Cantera	CEA Diff.	Cantera	CEA Diff.	Cantera	CEA Diff.
P (10^5 Pa)	8.3785	N/A	4.8249	0.37%	0.99181	0.01%
T (K)	3314.8	−0.09%	3151.2	−0.06%	2697.0	−0.09%
C_p (10^3 J/kg/K)	2.0771	−0.05%	2.0675	−0.07%	2.0325	0.09%
ρ (10^{-1} kg/m^3)	6.6174	0.06%	4.0651	0.39%	1.0093	0.07%
μ (10^{-5} Pa s)	9.4775	8.06%	9.1404	8.21%	8.1726	8.64%
k (10^{-1} W/m/K)	3.5689	−3.79%	3.3898	−3.55%	2.8982	−2.86%

All major species were found to have less than 1% difference in mole fractions between Cantera and CEA throughout the engine. Stagnation thermodynamic properties match very well, which is expected as GRI MECH uses the same thermodynamic data as CEA. Transport properties are consistently different; the empirical fits used by CEA are likely more accurate than the Lennard-Jones model used here, however the difference in calculated heat flux was found to be small.

3 Heat Transfer Correlations

It appears to be accepted to use the difference between the adiabatic wall temperature and the wall temperature as the driving potential for heat flux [8]–[10], so that was adopted here as well. The adiabatic wall temperature is given by:

$$T_{aw} = T + r(T_0 - T) \tag{5}$$

The recovery factor r is commonly given as:

$$r = (Pr)^{1/3} \tag{6}$$

The gas wall temperature was taken to be a constant value of 300K, as would be the case on engine startup. The influence of the gas wall temperature is discussed in Section 5.4.

When property evaluation at temperatures other than the free stream temperature is required, the gas temperature was changed in Cantera while keeping the pressure constant.

3.1 Bartz

The Bartz equation is commonly used for calculating rocket engine heat flux. The following form is common:

$$\begin{aligned} h_g &= \left[\frac{0.026}{D_t^{0.2}}\left(\frac{\mu^{0.2}c_p}{Pr^{0.6}}\right)_0\left(\frac{p_0}{c^*}\right)^{0.8}\left(\frac{D_t}{R_c}\right)^{0.1}\right]\left(\frac{A_t}{A}\right)^{0.9}\sigma \\ \sigma &= \frac{1}{\left[\frac{1}{2}\left(\frac{T_w}{T_0}\right)\left(1+\frac{\gamma-1}{2}M^2\right)+\frac{1}{2}\right]^{0.8-m/5}\left[1+\frac{\gamma-1}{2}M^2\right]^{m/5}} \end{aligned} \tag{7}$$

Here m is the exponent of the temperature dependence of viscosity, and it is commonly taken to be 0.6. The σ term accounts for property variation in the boundary layer and along the length of the engine.

If the equation is rearranged into nondimensional parameters the fact that it is a modified version of the Dittus-Boelter equation is more clear:

$$Nu_t = 0.026 Re_t^{0.8} Pr^{0.4}\left(\frac{D_t}{R_c}\right)^{0.1}\left(\frac{A_t}{A}\right)^{0.9}\sigma \tag{8}$$

Here all gas properties are evaluated at stagnation and the throat diameter is the characteristic dimension.

Another form given by Bartz also uses the stagnation gas properties but the characteristic dimension is the local diameter. It has a boundary layer property variation term that uses the gas viscosity and density at the arithmetic mean of the free stream and wall temperatures:

$$Nu_D = 0.026 Re_D^{0.8} Pr^{0.4}\left(\frac{D_t}{R_c}\right)^{0.1}\left[\left(\frac{\rho_{am}}{\rho}\right)^{0.8}\left(\frac{\mu_{am}}{\mu}\right)^{0.2}\right] \tag{9}$$

Three forms of the Bartz equation are graphed. The version with a property variation term (Equations 7 & 8) is shown based off of both purely CEA data with $m = 0.6$ and Cantera data where $m = 0.75$ was found to better fit the temperature dependence of the gas viscosity. The free stream version of Bartz (Equation 9) is also shown.

3.2 Dittus-Boelter

The unmodified Dittus-Boelter equation the Bartz equation is based on is given by:

$$Nu_D = 0.023 Re_D^{0.8} Pr^{0.4} \tag{10}$$

The Dittus-Boelter equation is known to be ill-suited to modeling flows with large property variations in the boundary layer [11]. A proposed solution is to evaluate all properties at the arithmetic mean of the free stream and wall temperatures [8], [10].

3.3 Sieder-Tate

When continuing with the theme of applying simple pipe-flow correlations to rocket engine heat transfer, the Sieder-Tate correlation seems relevant (as it is known for better modeling large property variations [11]). All properties are evaluated at the free stream temperature except for μ_w, which is evaluated at the wall temperature.

$$Nu_D = 0.027 Re_D^{0.8} Pr^{1/3} \left(\frac{\mu}{\mu_w} \right)^{0.14} \tag{11}$$

4 Calculated Heat Flux

The calculated heat flux using the methods described in Section 3 is shown in Figure 2.

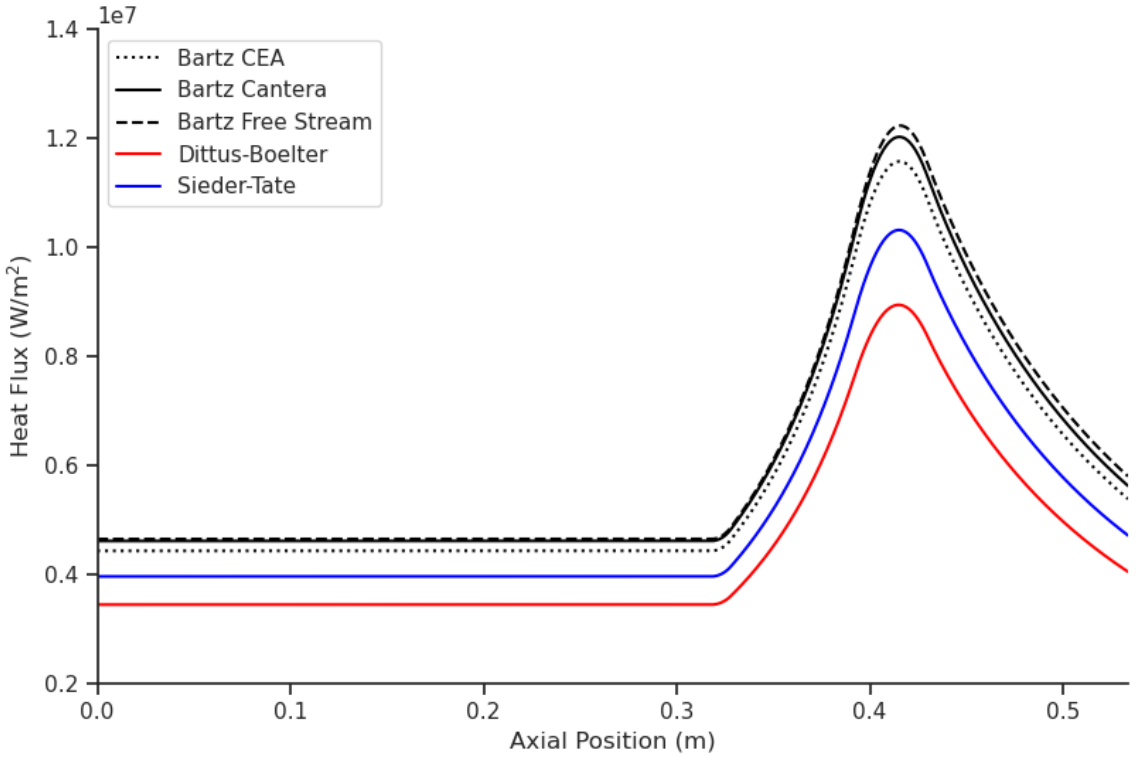

Figure 2: Calculated heat flux, OF=2.29.

The Bartz correlations all agree well and are within 5% of each other. The heat flux calculated with CEA values is the lower than the two Cantera curves — this is likely due to the difference in transport properties.

Despite directly applying the common Sieder-Tate equation to a rocket engine, it appears to match decently well with the Bartz values.

The largest difference was between the Dittus-Boelter and Bartz models, at 30%. This was found to be because of the difference in constants (11%), the throat curvature factor (10%), and the breakdown of the assumption of constant Prandtl number and specific heat (9%).

5 Modifying Factors

The free stream Bartz correlation (Equation 9) is used to illustrate the following effects.

5.1 OF Ratio

The OF Ratio can be reduced by keeping the total mass flow rate the same, or by decreasing the fuel flow rate. The effects of both are shown in Figure 3.

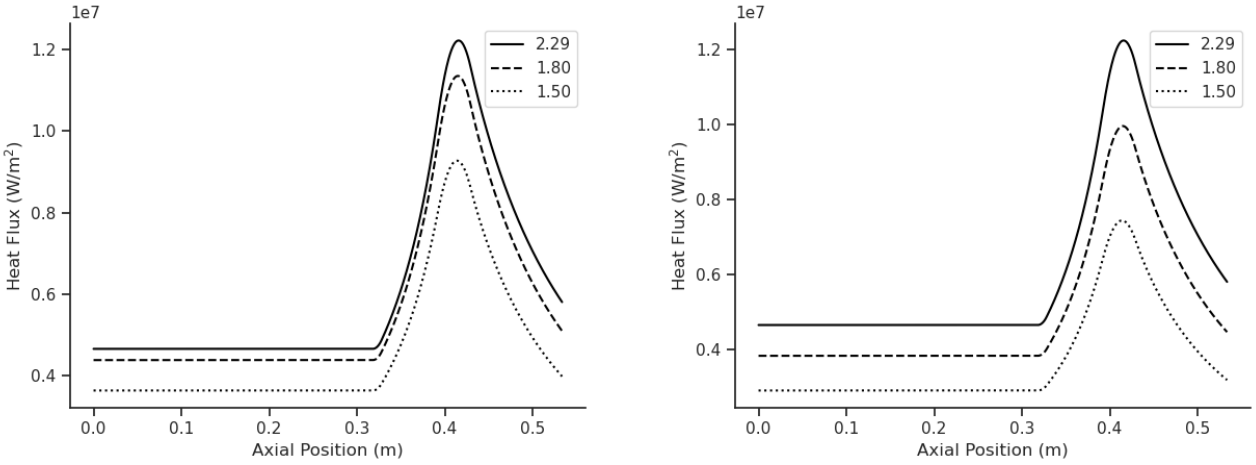

(a) Constant $\dot{m}$

(b) Variable $\dot{m}$

Figure 3: Effects of OF ratio on heat flux.

Other factors not accounted for here may make this difference more dramatic. At higher OF ratios the presence of dissociated species is greater, which can increase heat flux, and at lower OF ratios the effect of carbon deposition on the walls could be greater [12].

5.2 Frozen or Equilibrium Expansion

As noted before, the effects of assuming equilibrium or frozen expansion were found to be minor, and are shown in Figure 4. Reality would be somewhere in between these two extremes.

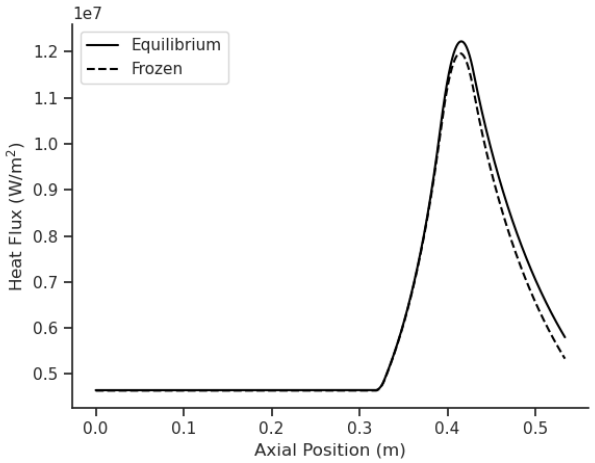

Figure 4: Heat flux with frozen and equilibrium expansion, OF=2.29.

5.3 Carbon Deposition

Carbon deposition can significantly decrease the heat flux into combustion walls [9, Page 86]. The material deposited has a very high thermal resistance and can reach high temperatures, reducing the temperature difference driving the heat flux into the walls. If the difference between the adiabatic wall temperature and the gas wall temperature is still used, then a modified heat transfer coefficient can be calculated from the thermal resistance of the deposit:

$$h_{gc} = \frac{1}{\frac{1}{h_g} + R} \tag{12}$$

The process is difficult to model and should be measured experimentally. It is generally accepted that deposition is lower for higher combustion gas mass fluxes (and therefore higher chamber pressures), and that it is lowest at the throat [9], [13]. The effect has been found to be greater at lower OF ratios [12]. Film cooling creates a region of low OF ratio near the walls, and can increase deposition [14, Page 35].

Masters et al [15] report an approximately 40% reduction in heat transfer coefficient at the throat for a LOX/RP-1 engine, and directly applying data for the thermal resistance of carbon deposits in a 7 MPa engine given by Huang and Hazel gives a reduction of around 60%.

Carbon layers can build up to their maximum thickness in 1 to 2 seconds [13], at which point they can become unstable and flake off [16]. This can lead to cyclic spikes in heat flux.

Studies on carbon deposition with high combustion efficiency ($> 94\%$) have found a lack of deposition [13], [17]. Makel suggests that deposition is caused by poor injector mixing efficiency causing regions of low mixture ratio. This is supported by chemical equilibrium calculations, which only show elemental carbon at very low mixture ratios. The effects of the pintle injector geometry and running fuel or oxidizer centered are likely worth looking into.

5.4 Wall Temperature

The maximum gas wall temperature can be found by assuming that the coolant wall is at the boiling temperature of the coolant. The boiling point of kerosene was found to be 618K (Section 6). A 1/16 inch steel wall was assumed, and the throat heat flux was iterated to find an equilibrium gas wall temperature of 897K. This represents the maximum gas wall temperature at the throat, elsewhere it would be lower.

Figure 5 shows the heat flux assuming a constant wall temperature of 897K. The throat heat flux was reduced by 28%.

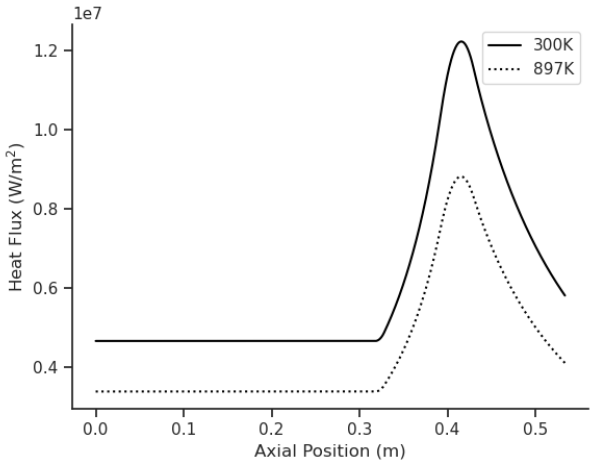

Figure 5: Heat flux at maximum wall temperature, OF=2.29.

5.5 Flow Recirculation

The recirculation zones that cause the famous combustion stability of pintle injectors can also cause higher chamber heat flux than predicted, as the combustion gas velocity near the wall can be much larger than the average cross-sectional velocity [8, Page 81].

A (very) simple estimate of this effect can be found by assuming that the combustion gas in the inner half of the radius flows towards the injector at the same velocity as the outer half of the radius, which flows towards the nozzle. It can be shown that this velocity must be twice the cross sectionally averaged velocity. Based off of the correlations in Section 3, this would increase the heat flux by 74%.

Bartz presents data for an Enzian injector, which features similar recirculation. The measured chamber heat flux is nearly 100% higher than predicted — surprisingly close to the crude estimate done here.

5.6 Combustion Efficiency

The previous results have all assumed perfect combustion performance. If the combustion efficiency is reduced, the chamber pressure and temperature would change, as well as species mole fractions.

From the correlations in Section 3 it can be seen that the heat transfer coefficient is proportional to the mass flux to the 0.8 power:

$$h_g \propto \left(\frac{\dot{m}}{A}\right)^{0.8} \tag{13}$$

The throat mass flux is more or less proportional to the chamber pressure:

$$\frac{\dot{m}}{A_t} = p_0 \sqrt{\frac{\gamma[2/(\gamma+1)]^{\frac{\gamma+1}{\gamma-1}}}{R_{gas} T_o}} \tag{14}$$

This leads to the oft-cited result that the throat heat flux is proportional to the chamber pressure to the 0.8 power. However, in the case of inefficient combustion, the chamber pressure would decrease, but the mass flux would stay the same. The largest reduction in heat flux would most likely come from the reduction in the combustion gas temperature.

The form of equation 7 is useful when looking at the influence of parameter changes. The gas specific heat and Prandtl number are relatively constant over a wide temperature range. The gas viscosity varies significantly, however it is only to power of 0.2. This indicates it would likely take a large reduction in combustion performance to produce a significantly lower heat flux than calculations assuming perfect combustion.

6 Regenerative Cooling

A simple analysis of the feasibility of regenerative cooling is conducted here.

Low thrust rocket engines are difficult to regeneratively cool. Thrust is proportional to the mass flow rate, and heat flux is proportional to the mass flow rate to the power of 0.8. This means that as engine thrust decreases the amount of coolant decreases faster than the heat flux.

In steady-state operation all the heat generated in the engine must be absorbed by the coolant without the free stream of the coolant exceeding its boiling temperature. If the coolant flow is capable of this, it only indicates that regenerative cooling is *technically* possible; unrealistic channel geometry may be required to keep the walls from melting. The details of channel geometry will be discussed separately.

Huber et al [18] developed a thermophysical model for RP-1 based on a surrogate mixture that they say is applicable up to temperatures of 800 K and pressures of 60 MPa. After reaching out to them, they provided files for the surrogate for use in NIST REFPROP [19].

The engine is divided into sections, and the heat flow into each section can be calculated from the heat flux and the internal surface area of the section. As the engine is in thermal equilibrium, all heat flow into each section must be taken out by the fuel, so the change in stagnation enthalpy at each station must be [20]

$$\Delta i = \frac{qA}{\dot{m}}, \tag{15}$$

where q is the heat flux at the start of the station, A is the area of the station, and $\dot{m}$ is the mass flow rate of the fuel. REFPROP data is then used to calculate the fuel temperature at each station.

Assuming a 20% pressure drop across the injector and a 15% pressure drop through the regenerative channels, the fuel input pressure was specified as 1.12 MPa. At this pressure, the fuel boiling temperature calculated by REFPROP is approximately 618K.

Chamber-only and nozzle-throat-only regenerative cooling were first studied separately using the Bartz heat flux, with the fuel input pressure and temperature at 1.12 MPa and 300K. With chamber-only cooling the fuel temperature increased by ~ 230 degrees, and with nozzle-throat-only cooling the fuel temperature increased by ~ 200 degrees. Regenerative cooling of the entire engine was only possible when the entire heat flux was scaled down by 25%.

Chamber-only cooling was not possible when the heat flux was increased by 75% to account for the possible increase due to recirculation.

7 Conclusion

On startup of the engine, the throat heat flux is predicted to be approximately 12 MW/m^2 and the chamber heat flux is predicted to range from 4.5 to 9 MW/m^2 depending on the significance of recirculation. If the combustion efficiency isn't too high, within 1 to 2 seconds a carbon layer could build up on the combustion walls, dramatically reducing the heat flux. Whether or not regenerative cooling is at all possible will likely depend on combustion gas recirculation and carbon buildup.

References

[1] S. Gorden and B. J. McBride, *Computer program for calculation of complex chemical equilibrium compositions and applications*, NASA Reference Publication 1311, 1996.

[2] S. Youngblood, "Design and testing of a liquid nitrous oxide and ethanol fueled rocket engine," Aug. 2015.

[3] T.-S. Wang, "Thermophysics characterization of kerosene combustion," *Journal of Thermophysics and Heat Transfer*, vol. 15, no. 2, pp. 140–147, Apr. 2001, ISSN: 0887-8722, 1533-6808. DOI: 10.2514/2.6602. [Online]. Available: https://arc.aiaa.org/doi/10.2514/2.6602 (visited on 08/16/2020).

[4] G. Smith and D. Golden. (). GRI-MECH 3.0, [Online]. Available: http://www.me.berkeley.edu/gri_mech/.

[5] B. J. McBride, M. Zehe, and S. Gordon, "NASA glenn coefficients for calculating thermodynamic properties of individual species," Sep. 2002.

[6] M. Martinez-Sanchez, *Reacting nozzle flow*.

[7] (). Cantera examples - sound speed, [Online]. Available: https://cantera.org/examples/python/thermo/sound_speed.py.html.

[8] D. Bartz, "Turbulent boundary-layer heat transfer from rapidly accelerating flow of rocket combustion gases and of heated air," in *Advances in Heat Transfer*, vol. 2, DOI: 10.1016/S0065-2717(08)70261-2, Elsevier, 1965, pp. 1–108, ISBN: 978-0-12-020002-3. [Online]. Available: https://linkinghub.elsevier.com/retrieve/pii/S0065271708702612 (visited on 07/26/2019).

[9] D. H. Huang and D. K. Huzel, *Modern Engineering for Design of Liquid-Propellant Rocket Engines*. Washington DC: American Institute of Aeronautics and Astronautics, Jan. 1992, DOI: 10.2514/4.866197, ISBN: 978-1-56347-013-4 978-1-60086-619-7. [Online]. Available: http://arc.aiaa.org/doi/book/10.2514/4.866197 (visited on 07/29/2019).

[10] W. M. Grisson, "Liquid film cooling in rocket engines," Arnold Engineering Development Center, Mar. 1991.

[11] T. L. Bergman and A. S. Lavine, *Fundamentals of heat and mass transfer*. 2017, OCLC: 1084350679, ISBN: 978-1-119-33010-3.

[12] R. Cook and R. Quentmeyer, "Advanced cooling techniques for high-pressure, hydrocarbon-fueled rocket engines," American Institute of Aeronautics and Astronautics, Jun. 30, 1980. DOI: 10.2514/6.1980-1266. [Online]. Available: http://arc.aiaa.org/doi/10.2514/6.1980-1266 (visited on 08/31/2020).

[13] D. Makel, "Carbon deposition model for oxygen/hydrocarbon combustion," May 1990.

[14] J. Campbell and D. Batha, "Thrust chamber cooling techniques for spacecraft engines," Feb. 1963.

[15] P. A. Masters and E. S. Armstrong, "High-pressure calorimeter chamber tests for liquid oxygen/kerosene (LOX/RP-1) rocket combustion," 1988.

[16] J. P. Sellers, "Effect of carbon deposition on heat transfer in a LOX/RP-1 thrust chamber," 1961.

[17] M. Lausten, D. Rousar, and S. Buccella, "Carbon deposition with LOX/RP-1 propellants," American Institute of Aeronautics and Astronautics, Jul. 8, 1985. DOI: 10.2514/6.1985-1164. [Online]. Available: http://arc.aiaa.org/doi/10.2514/6.1985-1164 (visited on 08/31/2020).

[18] M. L. Huber, E. W. Lemmon, L. S. Ott, and T. J. Bruno, "Preliminary surrogate mixture models for the thermophysical properties of rocket propellants RP-1 and RP-2," *Energy & Fuels*, vol. 23, no. 6, pp. 3083–3088, Jun. 18, 2009, ISSN: 0887-0624, 1520-5029. DOI: 10.1021/ef900216z. [Online]. Available: https://pubs.acs.org/doi/10.1021/ef900216z (visited on 05/10/2020).

[19] E. W. Lemmon, I. H. Bell, M. L. Huber, and M. O. McLinden, *NIST standard reference database 23: Reference fluid thermodynamic and transport properties-REFPROP*. 2018. [Online]. Available: https://www.nist.gov/srd/refprop.

[20] M. H. Naraghi and M. Foulon, "A simple approach for thermal analysis of regenerative cooling of rocket engines," ASMEDC, Jan. 1, 2008, pp. 531–538, ISBN: 978-0-7918-4871-5. DOI: 10.1115/IMECE2008-

67988. [Online]. Available: https://asmedigitalcollection.asme.org/IMECE/proceedings/IMECE2008/48715/531/332170 (visited on 05/10/2020).